Received 6 April 2023; revised 4 May 2023; accepted 9 May 2023. Date of publication 15 May 2023; date of current version 25 May 2023.

Digital Object Identifier 10.1109/OJAP.2023.3276686

Analytic Approximation of In-Body Path Loss for Implanted Antennas

MINGXIANG GAO [1], ZVONIMIR SIPUS [2] (Senior Member, IEEE), AND ANJA K. SKRIVERVIK [1]

[1] Microwaves and Antennas Group, Ecole Polytechnique Federale de Lausanne, 1015 Lausanne, Switzerland

[2] Faculty of Electrical Engineering and Computing, University of Zagreb, 10000 Zagreb, Croatia

CORRESPONDING AUTHOR: ANJA K. SKRIVERVIK (e-mail: anja.skrivervik@epfl.ch)

ABSTRACT Implantable bioelectronic devices predominantly use wireless links for communication and/or power transfer. When considering transmitting implanted antennas, electromagnetic radiation through biological media is highly attenuated, and previous work has shown that the in-body path loss can be separated into three parts: the losses incurred by the propagating fields, the reflections at media interfaces, and the coupling of the antenna reactive near field and the lossy body. The first two are unavoidable, but a careful antenna design should minimize the near-field losses. Thus, quantifying the near-field losses of implanted antennas is useful in selecting the antenna topology for preliminary design. The aim of this paper is to present a simplified model of an implanted antenna that provides closed-form approximate expressions to estimate EM radiation from the implant. In particular, we extend the expressions for the reactive near-field losses to both deep and shallow implants, by taking into account the implantation depth. Additionally, the proposed approximate method is verified by comparing the results obtained with the full-wave simulations in the case of a miniature implanted antenna, and with both simulated and measured results from two practical examples found in the literature.

INDEX TERMS Implanted antennas, in-body path loss, reactive near field, lossy medium.

I. INTRODUCTION

Implantable bioelectronic devices provide breakthrough capabilities for biomedical research and therapy [1], [2], [3], [4], [5]. Especially in the last decade, with the development of advanced materials and micro-fabrication technologies, wireless bioelectronics with implanted antennas are used in applications from implantable neural interfaces to wireless capsule endoscopy [6], [7], [8], [9], [10], [11], [12]. In biological science, advanced neuroengineering platforms have developed into long-lived neural interfaces with diverse operational modes, in which closed-loop operation through a wireless link becomes essential [12]. As an example of medical applications, wireless capsule endoscopy is used to record images of the digestive tract, where the high efficiency of the implanted antenna is a prerequisite for high-speed data transmission [13], [14], [15], [16]. Therefore, for most body-implanted devices, wireless communication and power transfer through the lossy body has become an indispensable requirement. To achieve an efficient wireless link, it becomes crucial to understand the loss mechanisms and quantify the inevitable losses from implanted antennas through the lossy biological tissues.

The radiation properties of arbitrary antennas in free space have been well investigated [17], [18], [19]. However, for antennas fully implanted in biological tissues, dissipation and scattering in the lossy host medium become the main cause of attenuation of the electromagnetic (EM) waves propagating in the body, resulting in low radiation efficiency [20], [21], [22]. Further studies have shown that the geometry and dimensions of the antenna encapsulation and host body greatly influence the antenna radiation properties. By looking into body phantoms with simplified geometries, such as spherical, cylindrical, or planar body models, the characteristics of implanted antennas can be analyzed from a macro perspective [23], [24], [25], [26], [27], [28], [29], [30], [31], [32], [33], [34]. Studies have been carried out to explore the physical limitations of implanted antennas and the optimum design of wireless body area networks.

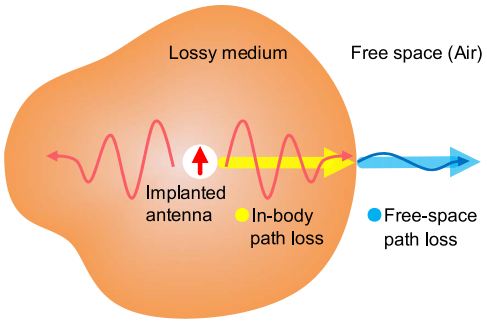

FIGURE 1. Sketch of an antenna implanted in a lossy medium.

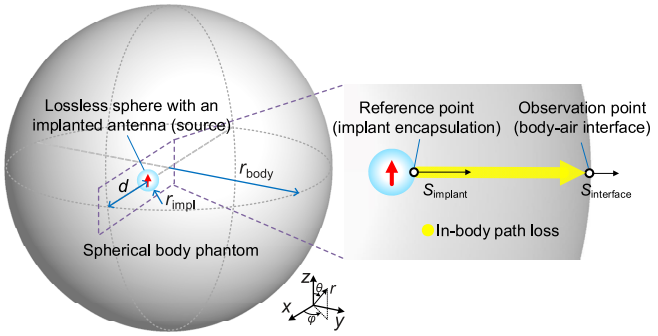

FIGURE 2. View of the spherical body model with an elementary dipole source implanted at a depth of *d*.

One research goal is to gain theoretical insight into the dissipation due to the lossy medium surrounding the antenna by establishing an analytic approximate method. In this way, it is possible to estimate quantitatively the losses caused by different mechanisms before starting a specific antenna design. This is critical as it provides guidelines and the scope of possible optimization (e.g., a quick link budget to estimate the minimum achievable in-body path loss) in the preliminary stages of implanted antenna design. In [32], the loss mechanisms for implanted antennas are analyzed, and the losses on the path from the implanted antenna to the body-air interface are divided into three main contributions: the losses due to the dissipation in the reactive near field, the propagating field absorption losses, and the losses due to reflections. The sketch in Fig. 1 shows visually where the losses occur for a typical implanted antenna.

According to the physical mechanisms causing the losses of implanted antennas, the antenna designer has little influence on propagating field absorption losses and reflection losses but an optimized design can significantly reduce the near-field losses. Thus, the latter requires a full understanding and quantitative estimation to set a benchmark for antenna design and optimization. The radian sphere as the boundary separating the near-field and far-field was first proposed in [35] and considered for tissue-implanted sources in [36]. Furthermore, the near-field characteristics of ideal dipoles in lossy media were analyzed regarding the total radiated power [37], leading to the conclusion that magnetic antennas are more efficient than electric ones once implanted in lossy media. To evaluate losses over the shortest wireless link, the in-body path loss (see Fig. 1) quantifies the attenuation in power density of EM waves propagating in the body, from the implanted antenna to the body–air interface [21], [38], [39], [40], [41]. In [32], approximate expressions of the in-body path loss are derived in order to determine the maximum power density reaching free space, including analytic approximations of the near-field losses of implanted antennas. The obtained expressions for the latter take into account key factors like the encapsulation size and the lossy medium into which the antenna is implanted, but does not include the implantation depth. In other words, it was assumed that the antenna is deeply implanted into the body. Furthermore, in the final approximate expressions only the dominant terms were taken into account, and the proposed expressions were validated only for the case of canonical dipole implanted antennas in spherical phantoms.

The aim of this paper is to present a simplified model of an implanted antenna that provides approximate analytic expressions for the EM radiation of the implant. In particular, we extend the expressions for the reactive near-field losses to take into account the implantation depth, in order to effectively consider both shallow and deep implants. Moreover, the proposed analytic approach is validated by comparison to full-wave simulation in the cases of a miniature implanted antenna and to simulated and measured results for two practical examples from the literature.

II. SIMPLIFIED MODEL DERIVATION

In order to derive approximate expressions, let us consider a canonical model: an elementary source placed in a spherical body phantom, as depicted in Fig. 2.

The implanted antenna, an elementary electric or magnetic dipole, is surrounded by a small air sphere, of radius r_{impl}, which roughly represents the dimension of the implant encapsulation. The source is implanted at a depth d within the spherical body phantom, the latter having variable radius r_{body}. To simulate the lossy biological tissue, the complex permittivity ε_{r} derived from the four-region Cole–Cole model [42] is applied to the medium of the body phantom. The phantom is set to be homogeneous to facilitate the initial analysis.

To characterize the losses of implanted antennas, the radiation efficiency and in-body path loss are two key performance indicators of interest [32]. The radiation efficiency provides a comprehensive indicator of the dissipated losses due to the presence of the lossy body. It is calculated as the ratio of the total radiated power reaching outside the body to the power entering the body medium through the encapsulation around the antenna. The in-body path loss, which is the protagonist of this paper, evaluates the path loss on the shortest wireless link from the source reaching the body–air interface. For most implantation scenarios, especially shallow implants, the in-body path loss is a practical indicator as it shows the minimum path loss from the implant through

the lossy host body, which is related to the upper limit of the link efficiency.

Using the spherical wave expansion (SWE) method [43], [44], [45], spherical body models were analyzed in [32], [33], [34]. On this basis, analytic approximations to assess the losses of implanted antennas are derived. As shown in [32] and [34], it is possible to decompose the in-body path loss using expressions for different contributions of losses (i.e., corresponding efficiency terms denoted as e):

$$\begin{aligned}\mathrm{Re}\{S_{\mathrm{interface}}\} &= \mathrm{Re}\{S_{\mathrm{implant}}\}\cdot\frac{r_{\mathrm{impl}}^2}{d^2}\cdot e_{\mathrm{total}}\\ &= \mathrm{Re}\{S_{\mathrm{implant}}\}\cdot\frac{r_{\mathrm{impl}}^2}{d^2}\cdot e_{\text{near field}}\\ &\quad\cdot e_{\mathrm{propagation}}\cdot e_{\mathrm{reflections}}.\end{aligned}\tag{1}$$

The power density of EM waves entering the body, $\mathrm{Re}\{S_{\mathrm{implant}}\}$, i.e., the maximum value of the real part of the Poynting vector component normal to the surface of the implant encapsulation, is set as the reference point for the in-body path loss. In the same way, the power density reaching the body–air interface is denoted as $\mathrm{Re}\{S_{\mathrm{interface}}\}$. These specific observation points evaluating the power density are depicted in Fig. 2. Note that the factor r_{impl}^2/d^2 accounts explicitly for the effect of the radial spreading of spherical EM waves, and thus the efficiency terms account for the losses in the host medium. In (1), the total in-body path loss is denoted as e_{total}, which can be divided into three efficiency terms. The first efficiency term $e_{\text{near field}}$ accounts for the losses due to the coupling of the implantable antenna's reactive near field with the lossy medium. The second term $e_{\mathrm{propagation}}$ represents the losses due to the propagating field and decays as $\exp[-2k''(d-r_{\mathrm{impl}})]$ (k'' is the linear attenuation coefficient of the host body medium). Finally, the third term $e_{\mathrm{reflections}}$ describes the reflection losses at the body–air interface, which is expressed in detail in [32].

If it is assumed that the source dipole is well matched and has no conductor losses or dielectric losses due to the encapsulation, the power density reaching the body–air interface can be expressed as

$$\mathrm{Re}\{S_{\mathrm{interface}}\} = P_{\mathrm{in}}\frac{1}{4\pi\, d^2}\cdot g_{\mathrm{Tx}}\cdot e_{\text{near field}}\cdot e_{\mathrm{propagation}}\cdot e_{\mathrm{reflections}},\tag{2}$$

where P_{in} is the input power and g_{Tx} is the gain of a short dipole in free space ($g_{\mathrm{Tx}} = 1.5$ or 1.76 dBi). Note that in some works, the gain of the antenna in lossy media is considered equivalent to the product of the antenna gain in free space and the efficiency due to reactive near-field losses. In this way, antenna-depended losses are included in the gain definition [24], [25], which is very useful in practice. This represents an additional demand for accurate analytic expressions for a quick estimation of the antenna gain in lossy media.

In this work, we focus on the approximations of the near-field term $e_{\text{near field}}$, since the other two terms are well understood [32], [34]. To distinguish $e_{\text{near field}}$ under different conditions, it is abbreviated in the rest of the paper as $e_{\text{near field}}^{\text{source type}}$. Here, the source type can be "TM" for electric dipole or "TE" for magnetic dipole. As discussed in [32], the lowest near-field losses are achieved if the implanted source excites only the fundamental spherical mode $n = 1$. On this basis, we first consider an electric dipole within a lossless capsule, which is placed in a homogenous lossy medium. The complex wave number of the lossy medium is $k = 2\pi\sqrt{\varepsilon_{\mathrm{r}}}/\lambda_0 = k' - ik''$, where λ_0 is the wavelength of EM waves in free space. The power density of EM fields excited by the source located in the origin of the spherical coordinate system can be expressed as

$$\begin{aligned}\mathrm{Re}\{S_r\} &= \mathrm{Re}\{E_\theta\cdot H_\varphi^*\}\\ &= \sum_{n,m}\frac{C_{\mathrm{mn}}}{r^2}\left[\frac{d}{\mathrm{d}\theta}P_n^{|m|}(cos\theta)\right]^2\mathrm{Re}\left[i\eta|k|^2\widehat{H}'^{(2)}_n(kr)\cdot\widehat{H}^{(2)*}_n(kr)\right]\\ &\overset{n=1}{=} C_{01}\frac{\sin^2\theta}{r^2}\mathrm{Re}\left\{\eta\left[|k|^2+2k''r^{-1}+\left(1-\frac{k^*}{k}\right)r^{-2}\right.\right.\\ &\qquad\left.\left.-ik^{-1}r^{-3}\right]\right\}\cdot\exp(-2k''r),\end{aligned}\tag{3}$$

where $\sum_{n,m} = \sum_{n=1}^{+\infty}\sum_{m=-n}^{n}$, m and n are the spherical mode indexes, C_{mn} are constants related to the corresponding spherical modal coefficients (in particular the constant C_{01} corresponds to the short dipole excitation and is determined by the power entering the lossy medium), P_n^m denotes the associated Legendre functions, and $\widehat{H}_n$ denotes the Schelkunoff spherical Hankel functions [44]. Note that in the polynomial inside the square brackets, the "near-field part" and the "far-field part" can be distinguished according to the knowledge of the radiative EM fields of the electric dipole in free space. Furthermore, the last term $\exp(-2k''r)$ is the one related to the losses due to the propagating field absorption.

Approximate expressions of $e_{\text{near field}}$ were first introduced in [32], assuming that the antenna is implanted deep enough in the body phantom to ensure that the reactive near fields do not reach free space.

However, for many implantation scenarios, the depth of the antenna is not large enough to ensure the near fields are completely attenuated before reaching free space. Indeed, the near-field region in the body depends on the electrical distance to the source (i.e., with respect to the wavelength λ_{body} in lossy tissue). It is worth noting that in the expression of total radiated power, the presence of near-field components at the body–air interface shows that part of the non-radiative reactive near field is transformed into radiated fields outside the lossy body. Thus, for cases with a relatively shallow implantation depth ($d \le \lambda_{\mathrm{body}}$), the approximate near-field losses should be modified to take into account the corresponding radiated power. Therefore, considering the implantation depth d, an accurate approximate expression can be derived for the excited spherical modes with index n

$$e_{\text{near field}}^{\mathrm{TM}} = \frac{\exp\left[2k''\left(d-r_{\mathrm{impl}}\right)\right]\mathrm{Re}\left[i\eta\widehat{H}'^{(2)}_n(kd)\cdot\widehat{H}^{(2)*}_n(kd)\right]}{\mathrm{Re}\left[i\eta\widehat{H}'^{(2)}_n\left(kr_{\mathrm{impl}}\right)\cdot\widehat{H}^{(2)*}_n\left(kr_{\mathrm{impl}}\right)\right]}.\tag{4}$$

For the fundamental spherical mode $n = 1$, the above expression can be written as

$$e^{\mathrm{TM}}_{\text{near field}} = \frac{\mathrm{Re}\left\{\eta\left[|k|^2 + 2k''d^{-1} + (1-k^*/k)d^{-2} - ik^{-1}d^{-3}\right]\right\}}{\mathrm{Re}\left\{\eta\left[|k|^2 + 2k''r_{\text{impl}}^{-1} + (1-k^*/k)r_{\text{impl}}^{-2} - ik^{-1}r_{\text{impl}}^{-3}\right]\right\}}. \quad (5)$$

It can be further approximated considering the dominant terms,

$$e^{\mathrm{TM}}_{\text{near field}} \approx \frac{\mathrm{Re}\left[\eta\left(|k|^2 - ik^{-1}d^{-3}\right)\right]}{\mathrm{Re}\left[\eta\left(|k|^2 - ik^{-1}r_{\text{impl}}^{-3}\right)\right]}. \quad (6)$$

With the same analysis procedure, for the magnetic dipole case with relatively shallow implantation depth ($d \le \lambda_{\text{body}}$), the approximate expression of near-field losses for the excited spherical modes with index n can be derived as

$$e^{\mathrm{TE}}_{\text{near field}} = \frac{\exp\left[2k''(d - r_{\text{impl}})\right]\mathrm{Re}\left[i\eta^{-1}\widehat{H}_n'^{(2)}(kd)\cdot\widehat{H}_n^{(2)*}(\mathrm{k\ d})\right]}{\mathrm{Re}\left[i\eta^{-1}\widehat{H}_n'^{(2)}(kr_{\text{impl}})\cdot\widehat{H}_n^{(2)*}(kr_{\text{impl}})\right]}. \quad (7)$$

Similarly, for the fundamental spherical mode $n = 1$, the above expression can be written as

$$\begin{aligned} e^{\mathrm{TE}}_{\text{near field}} &= \frac{\mathrm{Re}\left\{\eta^{-1}\left[|k|^2 + 2k''d^{-1} + (1-k^*/k)d^{-2} - ik^{-1}d^{-3}\right]\right\}}{\mathrm{Re}\left\{\eta^{-1}\left[|k|^2 + 2k''r_{\text{impl}}^{-1} + (1-k^*/k)r_{\text{impl}}^{-2} - ik^{-1}r_{\text{impl}}^{-3}\right]\right\}} \\ &= \frac{|k|^2 + 2k''d^{-1}}{|k|^2 + 2k''r_{\text{impl}}^{-1}}. \end{aligned} \quad (8)$$

It can be noted that in the final expression of (8), there are no higher-order terms of d or r_{impl}, which indicates that the magnetic dipole has much less power absorbed in the near-field region than the electric dipole. This is due to the fact that the near field of the magnetic dipole is essentially magnetic in nature, whereas the near field excited by electric dipoles is essentially electric in nature. The latter couples more strongly to biological tissues causing dielectric losses.

Using the proposed analytic approximation, the reactive near-field losses can be plotted as a function of the operating frequency and the implantation depth d. For instance, we consider here an implanted antenna with $r_{\text{impl}} = 1$ mm surrounded by muscle tissue. The near-field losses calculated by (5) and (8) for the electric dipole case and the magnetic dipole case are given in Fig. 3(a) and (b), respectively. The dielectric characteristics of the muscle tissue are obtained for each frequency using the Cole-Cole model [42]. Furthermore, at the operating frequency of 403.5 MHz and 2.45 GHz, these results are compared with the results calculated by the expressions of $e_{\text{near field}}$ in [32], as shown in Fig. 3(c) and (d). It can be seen that the near-field losses vary rapidly for small values of implanted antenna depth d, to finally tend to a constant value for a specific frequency when d is electrically large enough in the lossy medium; when this is not the case, especially for shallow implants, the effect of d becomes non-negligible. Compared to magnetic dipole cases, electric dipole cases have far more losses in the reactive near field, and the difference exceeds 10 dB when the frequency is below 1 GHz.

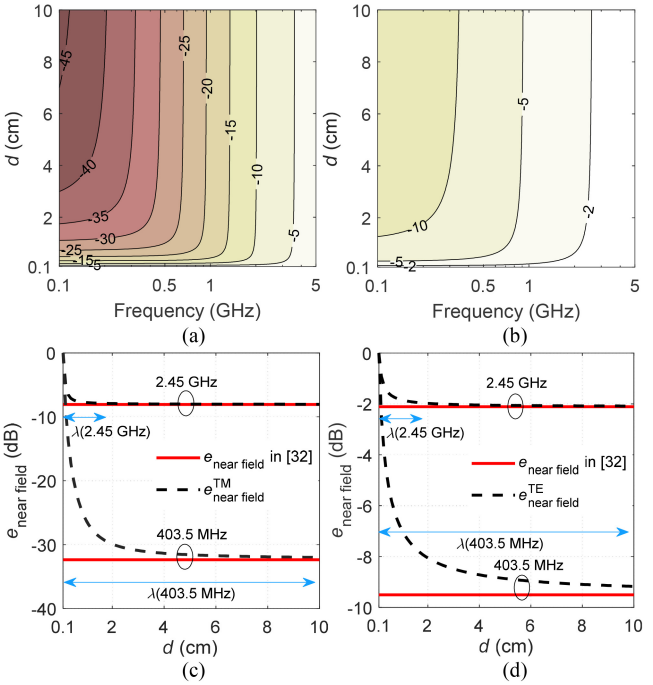

FIGURE 3. Distributions of the near-field losses (in dB) as a function of the frequency and d via the approximate expressions of (a) $e^{\mathrm{TM}}_{\text{near field}}$ and (b) $e^{\mathrm{TE}}_{\text{near field}}$. Comparisons of the near-field losses calculated using different approximate expressions for (c) electric dipole cases and (d) magnetic dipole cases.

III. VALIDATION AND APPLICATIONS

In this section, several realistic implanted antenna cases are analyzed to validate the analytic approximations, while demonstrating their use in assessing the in-body path loss.

A. SIMULATION ANALYSIS OF NEAR-FIELD PROPERTIES FOR AN IMPLANTED ANTENNA

To validate the usefulness of the proposed method in practical applications, a miniature implanted antenna is first investigated using full-wave simulation. As shown in Fig. 4, the cases where a capsule-shaped antenna is implanted in the center of a spherical body model and in a cubic body model are studied, respectively. The body phantoms in both models are made of muscle [42] with the antenna implantation depth of $r_{\text{body}} = d = 3$ cm, while the cubic body phantom has a side length $L_{\text{body}} = 15$ cm. This miniature implanted antenna is a short dipole antenna consisting of two conductor wires with a radius of $r_{\text{dip}} = 0.2$ mm, a feed gap of $g = 0.16$ mm, and an overall length of $L_{\text{dip}} = 2$ mm. To represent a general capsule encapsulation, the antenna is encapsulated in a lossless capsule filled by air, which is a cylinder (radius $r_{\text{encap}} = 1$ mm and length L_{dip}) terminated by two hemispherical ends with the same radius. According to the analysis of implanted capsules by Nikolayev et al. [31], the effective radius of the

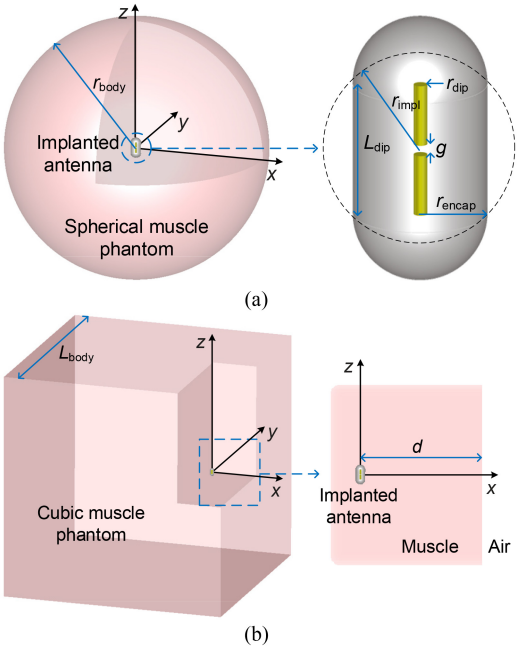

FIGURE 4. 3D View of the capsule-shaped implanted antenna models. (a) Spherical body model. (b) Cubic body model.

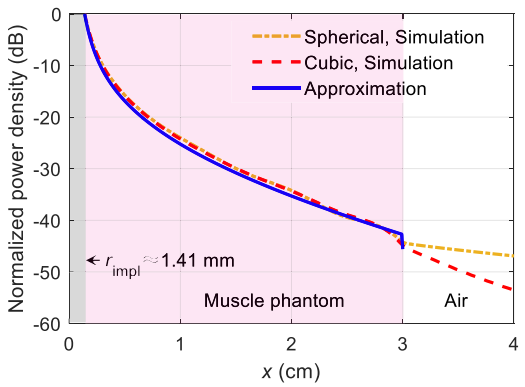

FIGURE 5. Normalized power density of EM waves propagating along the *x*-axis (shortest wireless path from implanted antenna to air) via the simulation solver and the approximate method.

implanted antenna r_{impl} (see Fig. 4) can be approximated by the circumradius of the encapsulation region containing the conductors, i.e., $r_{\text{impl}} \approx \sqrt{L_{\text{dip}}^2/4 + r_{\text{encap}}^2} \approx 1.41$ mm.

As shown in Fig. 4, the antenna is oriented in the z-direction (i.e., parallel to the nearest body–air interface) to maximize the link efficiency in the positive x-direction (i.e., perpendicular to the interface). This implanted antenna is simulated by an electromagnetic simulation solver (CST Microwave Studio 2019). For biomedical applications, the operating frequency of the antenna is 2.45 GHz, which is in one of the industrial, scientific, and medical (ISM) bands from 2.4 to 2.5 GHz. The power density of EM waves, as a function of the distance along the positive x-axis, is calculated using both the simulation solver and the proposed approximate method, as shown in Fig. 5.

TABLE 1. Simulated and approximate results for the maximum gain of the antenna in spherical body model.

Simulation	Approximation	
Maximum gain	e_{total}	Maximum gain
−18.50 dBi	−19.78 dB	−18.02 dBi

In the approximate method, we apply the two efficiency terms of the near-field losses and the propagating field losses within the body phantom (by replacing d with the variable x), and the term related to reflection losses is applied at the body–air interface (appears as a step drop at $x = d = 3$ cm). In both cases, the power density is normalized by the value at $x = r_{\text{impl}}$ as the reference value. Thus, the approximate expressions can be written as

$$\frac{\text{Re}\{S(x)\}}{\text{Re}\{S(r_{\text{impl}})\}} = \begin{cases} \frac{r_{\text{impl}}^2}{x^2} \cdot e_{\text{near field}}^{\text{TM}} \cdot e_{\text{propagation}}, & r_{\text{impl}} \le x < d \\ \frac{r_{\text{impl}}^2}{d^2} \cdot e_{\text{near field}}^{\text{TM}} \cdot e_{\text{propagation}} \cdot e_{\text{reflections}}, & x = d \end{cases}, \tag{9}$$

where $e_{\text{reflections}}$ represents the reflection losses at the body–air interface, which is calculated with spherical wave impedances in Fig. 5 corresponding to the spherical body model.

Within both spherical and cubic muscle body phantoms, i.e., 1.4 mm $\le x \le$ 3 cm in Fig. 5, specifically in the near-field region, the power densities obtained using both methods are almost overlapping, which validates the proposed approximation to the in-body path loss regardless of the phantom shape. For the shortest wireless path from the implanted antenna to the body–air interface, the proposed approximate method can effectively assess the in-body losses of power density (within 1.5 dB deviation from the simulation results for both cases). For the power density of EM waves propagating outside the body phantom, its attenuation is known as the free-space path loss, which is a function of distance, operating frequency, and the curvature radius of the body–air interface (the interface can be regarded as a radiating aperture according to the equivalence principle).

In particular, for the spherical body model, the radiated EM waves propagate to free space and maintain spherical symmetry throughout. In Fig. 5, it is observed that the power density of the spherical model case decays more slowly in free space than that of the cubic one, i.e., it only decays by the radial spreading factor $1/4\pi d^2$. In this principle, the far-field gain of this implanted antenna is only attenuated by the in-body path loss e_{total}. To convert e_{total} to a gain value in dBi, its value needs to be enlarged by 1.76 dB, which is the directivity of an electrically short dipole. Ultimately, the difference between the approximate and simulated results of the maximum far-field gain of the antenna is within 0.5 dB (see Table 1).

B. LINK PATH LOSS FOR A WIRELESS CAPSULE ENDOSCOPY SYSTEM

The proposed method provides an analytic approximation to directly estimate the link path loss from the implanted

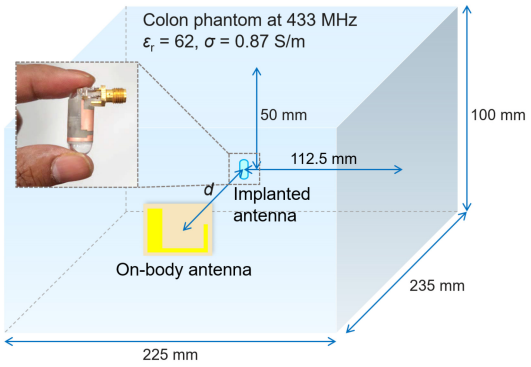

FIGURE 6. Measurement setup for link path loss of the in-body to on-body radio link. This figure is redrawn according to [46].

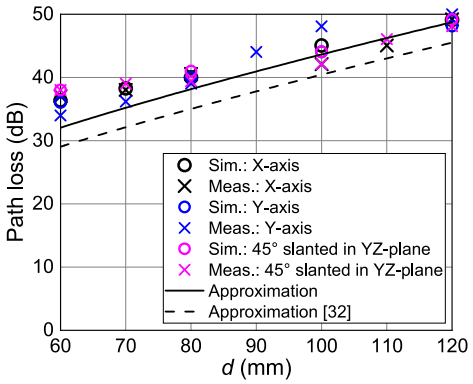

FIGURE 7. Simulated and measured results of link path loss between the in-body capsule and on-body antennas obtained from [46, Fig. 21], which are in good agreement with the approximate results (solid black curve).

antenna to an on-body antenna placed on the body-air interface. To illustrate its usefulness, we take a wireless capsule endoscopy system previously described in [46] as an example.

A novel capsule endoscope antenna was developed and presented in [46]. It consists of a loop antenna patterned on a flexible substrate and encapsulated by a polystyrene capsule module. Detailed dimensions can be found in [46, Table 3]. Based on the method presented in Section II, the effective radius of this antenna r_{impl} can be expressed as $r_{\text{impl}} \approx \sqrt{12.5^2/4 + 5.5^2} \approx 8.33$ mm, where 12.5 mm is the length of the antenna and 5.5 mm is the capsule radius. The *in vitro* measurement setup for the link path loss between the in-body capsule and on-body antennas is described in [46] and illustrated in Fig. 6. To model the lossy biological tissue, the homogeneous colon tissue body phantom was used both in simulations and measurements in [46], where its permittivity is given. A receiver antenna (a meandered monopole antenna) was placed in the center of the outer wall of the body phantom as an on-body antenna. The operating frequency of the wireless system is 433 MHz.

By changing the distance d between the capsule antenna and the on-body antenna, the link path loss was simulated and measured in [46], as shown in Fig. 7. According to the definition of total in-body path loss e_{total} in (1), the transmission coefficient between the implanted antenna and an on-body antenna can be derived in the following way:

$$|S_{21}|^2 = \frac{g_{\text{Tx}} A_{\text{e}}}{4\pi d^2} e_{\text{total}}, \tag{10}$$

where A_e is the effective aperture of the on-body antenna [25], i.e., $A_e = g_{\text{Rx}} \lambda_{\text{body}}{}^2/4\pi$. Specifically, g_{Rx} is the gain of the on-body monopole antenna and λ_{body} is the wavelength in the lossy colon body phantom. As in [46], the link path loss of this two-port network can be evaluated in decibels as $-10 \log_{10} |S_{21}|^2$.

Considering that the implanted antenna is a capsule loop antenna (i.e., magnetic-type antenna), the expression of $e^{\text{TE}}_{\text{NF,shallow}}$ is used in assessing the near-field losses. As a consequence, the link path loss as a function of the distance d is analytically approximated, as shown by the solid black curve in Fig. 7. Overall, approximate results demonstrate their close agreement (most deviations are less than 3 dB) with the simulated and measured results in all the tested capsule orientations. Note that using (10) to approximate $|S_{21}|$ is no longer applicable for very short distances, especially when d is smaller than the size of the on-body antenna. This is due to the non-uniform distribution of the power density reaching the on-body antenna, which leads to errors in the effective aperture estimation. In addition, the approximation to the maximum power density given in [32] (i.e., expressions [32, eqs. (22) and (24)]) can also achieve a rough estimate of the link path loss after a similar derivation of $|S_{21}|$, as shown by the black dashed line in Fig. 7. Since in these approximate expressions only the dominant terms are taken into account, the path loss results are underestimated by around 3 dB compared to the results of the proposed approximation.

C. FAR-FIELD GAIN FOR A CAPSULE ANTENNA WITHIN A SPHERICAL BODY PHANTOM

The proposed closed-form expressions were validated using a second example from the literature [47], depicted in Fig. 8. It consists of a dual-band antenna working at 434 MHz and 2.45 GHz, encapsulated in a lossless cylinder and placed at the center of a spherical glass container of φ100 mm filled with a liquid having dielectric properties equivalent to muscle. All dimensions and details can be found in [47]. The far-field gain of the antenna located in a spherical body phantom is both simulated and measured in [47].

In the following, we calculate the same gain using the following considerations: As the body phantom is a sphere and the antenna is placed in its center, the only attenuation of the power density incurred by the fields after reaching the sphere-free space interface is the radial spreading. Thus, the radiation pattern of the antenna in the sphere is identical to the radiation pattern of the same antenna radiating directly into free space. The gain system consisting of the antenna placed in the sphere can thus be written as $g = g_{\text{free space}} \cdot e_{\text{total}}$, where e_{total} is defined in (1). As the

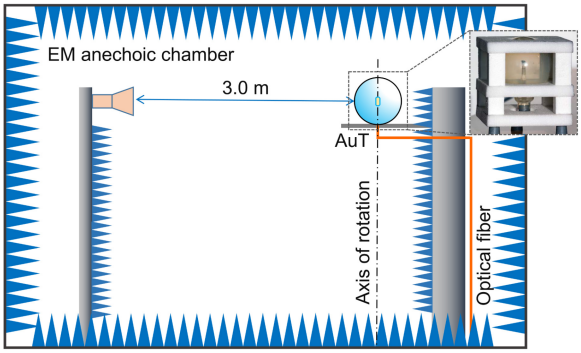

FIGURE 8. Measurement setup for far-field gain in an anechoic chamber, in which the antenna under test (AuT) is located inside a glass spherical container filled with a liquid body phantom. This figure is redrawn according to [47].

TABLE 2. Simulated, measured, and approximate results of far-field gain for a capsule antenna within a spherical phantom.

Frequency	Simulation [47]	Measurement [47]	Approximation	Approximation [32]
434 MHz	–28.9 dBi	–29.3 dBi	–27.63 dBi	–25.13 dBi
2.45 GHz	–18.6 dBi	–22.1 dBi	–18.72 dBi	–18.77 dBi

antenna is electrically small and basically omnidirectional, the free-space gain of the antenna $g_{\text{free space}}$ can be taken as 1.76 dBi, which is the gain of a Hertzian dipole.

To calculate $e_{\text{near field}}$ using the expressions described in Section II, we need to determine if the antenna radiates an electric or a magnetic type of mode. The antenna current distribution analysis provided in [47, Fig. 2] shows that the mode is the electric type (TM_{10}). Moreover, we can compute the effective radius of a spherical encapsulation equivalent to the original cylindrical in [47] using the method described in [31]. We obtain $r_{\text{impl}} \approx \sqrt{13.5^2/4 + 4.5^2} \approx 8.11$ mm at 434 MHz, where 13.5 mm is the length of the primary radiating elements Z_2 and 4.5 mm is the capsule radius (see [47, Figs. 1 and 2]). At 2.45 GHz, the effective radius of this antenna r_{impl} changes to $r_{\text{impl}} \approx \sqrt{8.1^2/4 + 4.5^2} \approx 6.05$ mm, where 8.1 mm is the length of the primary radiating element Z_3. The implantation depth is given by the radius of the spherical container, i.e., 50 mm.

The gain obtained using the approximation for the near-field losses presented in Section II is compared to the measured and simulated gain from [47] in Table 2. Overall, for both frequencies, the results obtained using the proposed approximate expressions agree well with the full-wave simulation results of [47]. The slight discrepancy with the measured results is, according to [47], due mainly to fabrication tolerances. The last column of Table 2 demonstrates the results using the approximation to the maximum power density given in [32]. The expressions in [32] were developed for deep implants and the dominant terms only were taken into account. In this example, the results are not very different from those by the proposed method, as the antenna is electric type and the implant is relatively deep. As the electrical length of the implantation depth decreases for the low-frequency band 434 MHz, the difference widens by more than –2 dB due to the larger error in the approximation of near-field losses.

IV. CONCLUSION

In this work, closed-form approximate expressions are derived for estimating the in-body path loss for antennas implanted in lossy media such as biological tissues, addressing more specifically the near-field losses. The latter losses depend heavily on the considered antenna and implantation depth. The proposed expressions give a quick assessment of the inevitable losses due to the lossy medium over the shortest wireless link and can be valuable in the initial design stages of an implanted antenna.

Among the different loss mechanisms, the coupling of the antenna reactive near field and the lossy body is a crucial part to be considered, as it is the only loss contribution that can be improved through careful antenna design without changing the implantation environment/host body. The obtained approximate expressions are applicable for both deep and shallow implantation scenarios and they distinguish the near-field losses for any given spherical wave mode. Specific expressions for the fundamental mode $n = 1$ are fully analyzed, as they yield the lowest achievable near-field losses among the various excitation modes and thus represent a useful benchmark.

The proposed approximate expressions are validated by comparing full-wave simulations of two implanted antenna cases, where good agreement is achieved for the near-field properties. Two realistic implanted antenna cases from previous literature are further discussed using our method to obtain the path loss, and an excellent agreement between our approximated results and the full-wave simulations and measurements from the literature are observed.

ACKNOWLEDGMENT

The authors acknowledge with gratitude the assistance from Hannes Bartle and Ismael Vico Trivino in the simulation analysis.

REFERENCES

[1] D. Fitzpatrick, *Implantable Electronic Medical Devices*. New York, NY, USA: Elsevier, 2014.
[2] E. Katz, *Implantable Bioelectronics*. Weinheim, Germany: Wiley, 2014.
[3] K. Agarwal, R. Jegadeesan, Y.-X. Guo, and N. V. Thakor, "Wireless power transfer strategies for implantable bioelectronics," *IEEE Rev. Biomed. Eng.*, vol. 10, pp. 136–161, 2017.
[4] Y. Li, N. Li, N. De Oliveira, and S. Wang, "Implantable bioelectronics toward long-term stability and sustainability," *Matter*, vol. 4, no. 4, pp. 1125–1141, 2021.
[5] G. Schiavone et al., "Soft, implantable bioelectronic interfaces for translational research," *Adv. Mater.*, vol. 32, no. 17, 2020, Art. no. 1906512.
[6] K. L. Montgomery et al., "Wirelessly powered, fully internal optogenetics for brain, spinal and peripheral circuits in mice," *Nat. Methods*, vol. 12, no. 10, pp. 969–974, Oct. 2015.
[7] K. N. Noh et al., "Miniaturized, battery-free optofluidic systems with potential for wireless pharmacology and optogenetics," *Small*, vol. 14, no. 4, 2018, Art. no. 1702479.

[8] Z. Xie, R. Avila, Y. Huang, and J. A. Rogers, "Flexible and stretchable antennas for biointegrated electronics," *Adv. Mater.*, vol. 32, no. 15, 2020, Art. no. 1902767.
[9] G. L. Barbruni, P. M. Ros, D. Demarchi, S. Carrara, and D. Ghezzi, "Miniaturised wireless power transfer systems for neurostimulation: A review," *IEEE Trans. Biomed. Circuits Syst.*, vol. 14, no. 6, pp. 1160–1178, Dec. 2020.
[10] N. A. Malik, P. Sant, T. Ajmal, and M. Ur-Rehman, "Implantable antennas for bio-medical applications," *IEEE J. Electromagn. RF Microw. Med. Biol.*, vol. 5, no. 1, pp. 84–96, Mar. 2021.
[11] A. Kiourti et al., "Next-generation healthcare: Enabling technologies for emerging bioelectromagnetics applications," *IEEE Open J. Antennas Propag.*, vol. 3, pp. 363–390, 2022.
[12] S. M. Won, L. Cai, P. Gutruf, and J. A. Rogers, "Wireless and battery-free technologies for neuroengineering," *Nat. Biomed. Eng.*, vol. 7, pp. 405–423, Apr. 2023.
[13] A. Kiourti, K. A. Psathas, and K. S. Nikita, "Implantable and ingestible medical devices with wireless telemetry functionalities: A review of current status and challenges," *Bioelectromagnetics*, vol. 35, no. 1, pp. 1–15, Jan. 2015.
[14] D. Nikolayev, M. Zhadobov, L. L. Coq, P. Karban, and R. Sauleau, "Robust ultraminiature capsule antenna for ingestible and implantable applications," *IEEE Trans. Antennas Propag.*, vol. 65, no. 11, pp. 6107–6119, Nov. 2017.
[15] J. Faerber et al., "*In vivo* characterization of a wireless telemetry module for a capsule endoscopy system utilizing a conformal antenna," *IEEE Trans. Biomed. Circuits Syst.*, vol. 12, no. 1, pp. 95–105, Feb. 2017.
[16] Z. Bao, Y.-X. Guo, and R. Mittra, "Conformal capsule antenna with reconfigurable radiation pattern for robust communications," *IEEE Trans. Antennas Propag.*, vol. 66, no. 7, pp. 3354–3365, Jul. 2018.
[17] H. A. Wheeler, "Fundamental limitations of small antennas," *Proc. IRE*, vol. 35, no. 12, pp. 1479–1484, Dec. 1947.
[18] L. J. Chu, "Physical limitations of omni-directional antennas," *J. Appl. Phys.*, vol. 19, no. 12, pp. 1163–1175, 1948.
[19] R. F. Harrington, "On the gain and beamwidth of directional antennas," *IRE Trans. Antennas Propag.*, vol. AP-6, no. 3, pp. 219–225, 1958.
[20] P. Hall and Y. Hao, *Antennas and Propagation for Body-Centric Wireless Communications*, 2nd ed. Norwood, MA, USA: Artech House, 2012.
[21] P. A. Floor et al., "In-body to on-body ultrawideband propagation model derived from measurements in living animals," *IEEE J. Biomed. Health Informat.*, vol. 19, no. 3, pp. 938–948, May 2015.
[22] L. Berkelmann and D. Manteuffel, "Characterization of wearable and implanted antennas: Test procedure and range design," *IEEE Trans. Antennas Propag.*, vol. 70, no. 4, pp. 2593–2601, Apr. 2022.
[23] J. Kim and Y. Rahmat-Samii, "Implanted antennas inside a human body: Simulations, designs, and characterizations," *IEEE Trans. Microw. Theory Techn.*, vol. 52, no. 8, pp. 1934–1943, Aug. 2004.
[24] A. Karlsson, "Physical limitations of antennas in a lossy medium," *IEEE Trans. Antennas Propag.*, vol. 52, no. 8, pp. 2027–2033, Aug. 2004.
[25] J. Lee and S. Nam, "Effective area of a receiving antenna in a lossy medium," *IEEE Trans. Antennas Propag.*, vol. 57, no. 6, pp. 1843–1845, Jun. 2009.
[26] A. S. Y. Poon, S. O. Driscoll, and T. H. Meng, "Optimal frequency for wireless power transmission into dispersive tissue," *IEEE Trans. Antennas Propag.*, vol. 58, no. 5, pp. 1739–1750, May 2010.
[27] F. Merli, B. Fuchs, J. R. Mosig, and A. K. Skrivervik, "The effect of insulating layers on the performance of implanted antennas," *IEEE Trans. Antennas Propag.*, vol. AP-59, no. 1, pp. 21–31, Jan. 2011.
[28] A. Kiourti and K. S. Nikita, "Implantable antennas: A tutorial on design, fabrication, and *in vitro*/*in vivo* testing," *IEEE Microw. Mag.*, vol. 15, no. 4, pp. 77–91, Jun. 2014.
[29] M. Bosiljevac, Z. Šipuš, and A. K. Skrivervik, "Propagation in finite lossy media: An application to WBAN," *IEEE Antennas Wireless Propag. Lett.*, vol. 14, pp. 1546–1549, 2015.
[30] D. P. Chrissoulidis and J.-M. Laheurte, "Radiation from an encapsulated Hertz dipole implanted in a human torso model," *IEEE Trans. Antennas Propag.*, vol. 64, no. 12, pp. 4984–4992, Dec. 2016.
[31] D. Nikolayev, W. Joseph, M. Zhadobov, R. Sauleau, and L. Martens, "Optimal radiation of body-implanted capsules," *Phys. Rev. Lett.*, vol. 122, no. 10, Mar. 2019, Art. no. 108101.
[32] A. Skrivervik, M. Bosiljevac, and Z. Šipuš, "Fundamental limits for implanted antennas: Maximum power density reaching free space," *IEEE Trans. Antennas Propag.*, vol. 67, no. 8, pp. 4978–4988, Aug. 2019.
[33] M. Gao, D. Nikolayev, M. Bosiljevac, Z. Šipuš, and A. K. Skrivervik, "Rules of thumb to assess losses of implanted antennas," in *Proc. 15th Eur. Conf. Antennas Propag (EuCAP)*, Mar. 2021, pp. 1–5.
[34] M. Gao, Z. Šipuš, and A. K. Skrivervik, "On the maximum power density of implanted antennas within simplified body phantoms," in *Proc. 16th Eur. Conf. Antennas Propag. (EuCAP)*, Madrid, Spain, 2022, pp. 1–5.
[35] H. A. Wheeler, "The radiansphere around a small antenna," *Proc. IRE*, vol. 47, no. 8, pp. 1325–1331, Aug. 1959.
[36] Y. El-Saboni, D. E. Zelenchuk, G. A. Conway, and W. G. Scanlon, "Assessing the intrinsic radiation efficiency of tissue-implanted UHF antennas," *IEEE Trans. Antennas Propag.*, vol. 68, no. 1, pp. 491–499, Jan. 2020.
[37] M. Manteghi and A. A. Y. Ibraheem, "On the study of the near-fields of electric and magnetic small antennas in lossy media," *IEEE Trans. Antennas Propag.*, vol. 62, no. 12, pp. 6491–6495, Dec. 2014.
[38] D. B. Smith, D. Miniutti, T. A. Lamahewa, and L. W. Hanlen, "Propagation models for body-area networks: A survey and new outlook," *IEEE Antennas Propag. Mag.*, vol. 55, no. 5, pp. 97–117, Oct. 2013.
[39] D. Kurup, G. Vermeeren, E. Tanghe, W. Joseph, and L. Martens, "In-to out body antenna-independent path loss model for multilayered tissues and heterogeneous medium," *Sensors*, vol. 15, no. 1, pp. 408–421, 2015.
[40] R. Chávez-Santiago et al., "Experimental path loss models for inbody communications within 2.36-2.5 GHz," *IEEE J. Biomed. Health Informat.*, vol. 19, no. 3, pp. 930–937, May 2015.
[41] S. Ullah, M. Zada, A. Basir, and H. Yoo, "Wireless, battery-free, and fully implantable micro-coil system for 7 T brain MRI," *IEEE Trans. Biomed. Circuits Syst.*, vol. 16, no. 3, pp. 430–441, Jun. 2022.
[42] S. Gabriel, R. W. Lau, and C. Gabriel, "The dielectric properties of biological tissues: III. Parametric models for the dielectric spectrum of tissues," *Phys. Med. Biol.*, vol. 41, no. 11, pp. 2271–2293, 1996.
[43] J. A. Stratton, *Electromagnetic Theory*. New York, NY, USA: McGraw-Hill, 1941.
[44] R. F. Harrington, *Time-Harmonic Electromagnetic Fields*. New York, NY, USA: McGraw-Hill, 1961.
[45] S. Stein, "Addition theorems for spherical wave functions," *Quart. Appl. Math.*, vol. 19, no. 1, pp. 15–24, 1961.
[46] M. S. Miah, A. N. Khan, C. Icheln, K. Haneda, and K.-I. Takizawa, "Antenna system design for improved wireless capsule endoscope links at 433 MHz," *IEEE Trans. Antennas Propag.*, vol. 67, no. 4, pp. 2687–2699, Apr. 2019.
[47] D. Nikolayev, A. K. Skrivervik, J. S. Ho, M. Zhadobov, and R. Sauleau, "Reconfigurable dual-band capsule-conformal antenna array for in-body bioelectronics," *IEEE Trans. Antennas Propag.*, vol. 70, no. 5, pp. 3749–3761, May 2022.

MINGXIANG GAO received the double B.Sc. degree in electrical engineering and business administration and the first M.Sc. degree in electrical engineering from Xi'an Jiaotong University, Xi'an, China, in 2016 and 2019, respectively, and the second M.Sc. degree (summa cum laude) in electrical engineering from the Politecnico di Milano, Milan, Italy, in 2019. He is currently pursuing the Ph.D. degree in electrical engineering with the Ecole Polytechnique Fédérale de Lausanne, Lausanne, Switzerland. His current research interests include the theory and design of implantable antennas, wireless techniques for bioelectronics, and bioelectromagnetics.

ZVONIMIR SIPUS (Senior Member, IEEE) received the B.Sc. and M.Sc. degrees in electrical engineering from the University of Zagreb, Zagreb, in 1988 and 1991, respectively, and the Ph.D. degree in electrical engineering from the Chalmers University of Technology, Gothenburg, Sweden, in 1997. From 1988 to 1994, he was with Rudjer Boskovic Institute, Zagreb, as a Research Assistant, where he was involved in the development of detectors for explosive gasses. In 1994, he joined the Antenna Group, Chalmers University of Technology, where he was involved in research projects concerning conformal antennas and soft and hard surfaces. In 1997, he joined the Faculty of Electrical Engineering and Computing, University of Zagreb, where he is currently a Professor. From 1999 to 2005, he was also an Adjunct Researcher with the Department of Electromagnetics, Chalmers University of Technology. Since 2006, he has been involved in teaching with the European School of Antennas. From 2008 to 2012 and from 2014 to 2018, he was the Head of the Department of Wireless Communications. His current research interests include the analysis and design of electromagnetic structures with application to antennas, microwaves, and optical communication and sensor systems.

ANJA K. SKRIVERVIK received the master's degree in electrical engineering and the Ph.D. degree from the Ecole Polytechnique Fédérale de Lausanne (EPFL), Lausanne, Switzerland, in 1986 and 1992, respectively. She was an Invited Research Fellow with the University of Rennes, Rennes, France, followed by two years in the industry. In 1996, she rejoined EPFL as an Assistant Professor, where she is currently a Full Professor and also the Head of the Microwaves and Antennas Group. She was the Director of the EE section from 1996 to 2000, and is currently the Director of the EE Doctoral School with EPFL. Her teaching activities include courses on microwaves and antennas and courses at Bachelor, Master, and Ph.D. levels. She has authored or coauthored more than 200 peer-reviewed scientific publications. Her current research interests include electrically small antennas, antennas in biological media, multifrequency and ultrawideband antennas, and numerical techniques for electromagnetics. She was the recipient of the Latsis Award. She is frequently requested to review research programs and centres in Europe. She was the Chairperson of the Swiss URSI until 2012. She is very active in European collaboration and European Projects. Since 2017, she has been a member of the Board of Directors of the European Association on Antennas and Propagation and is a Board Member of the European School on Antennas.